

## Supporting Information

### Pentacoordinated Al<sup>3+</sup> stabilized polyoxometalates for the efficient catalytic valorization of biomass-derived feedstocks

Lihua Wang<sup>a</sup>, Shuangxiu Ma<sup>a</sup>, Chunhong Chen<sup>a</sup>, Bing Lu<sup>a</sup>, Zhe Wang<sup>a</sup>, Yong Wang<sup>a</sup>, and Shanjun Mao<sup>\*a</sup>

<sup>a</sup>Advanced Materials and Catalysis Group, Center of Chemistry for Frontier Technologies, State Key Laboratory of Clean Energy Utilization, Institute of Catalysis, Department of Chemistry, Zhejiang University, Hangzhou 310028, P. R. China

\*Corresponding author: maoshanjun@zju.edu.cn (Shanjun Mao)

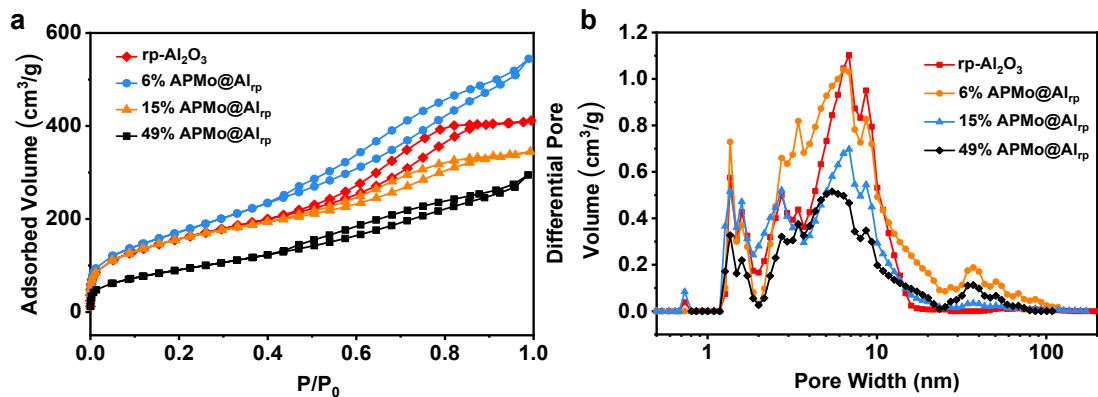


**Fig. S1.** (a)  $\text{N}_2$  adsorption and desorption isotherms, and (b) Pore size distributions of the catalysts.

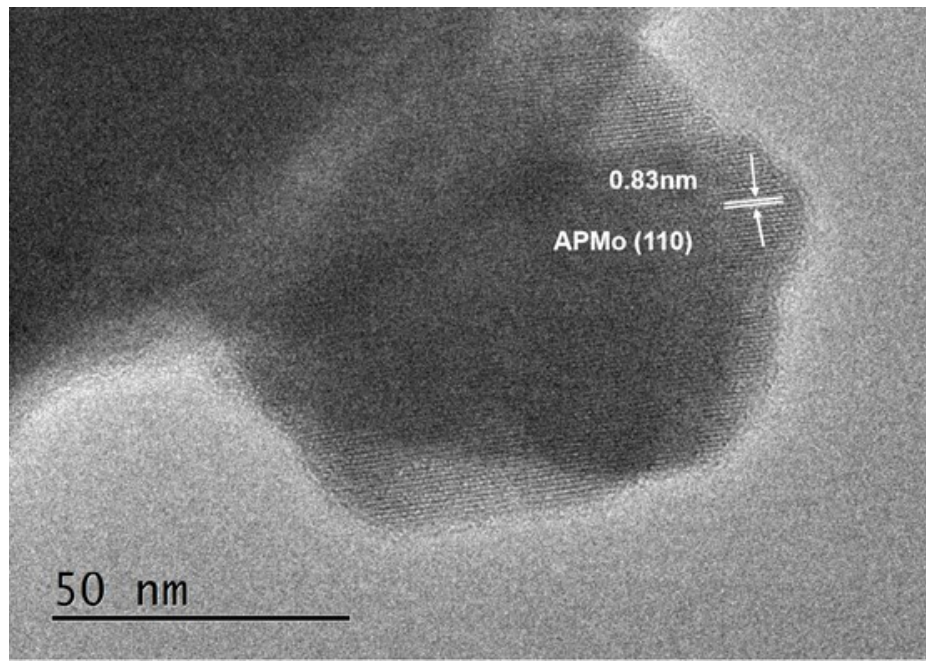


**Fig. S2.** HRTEM image of pure APMo.

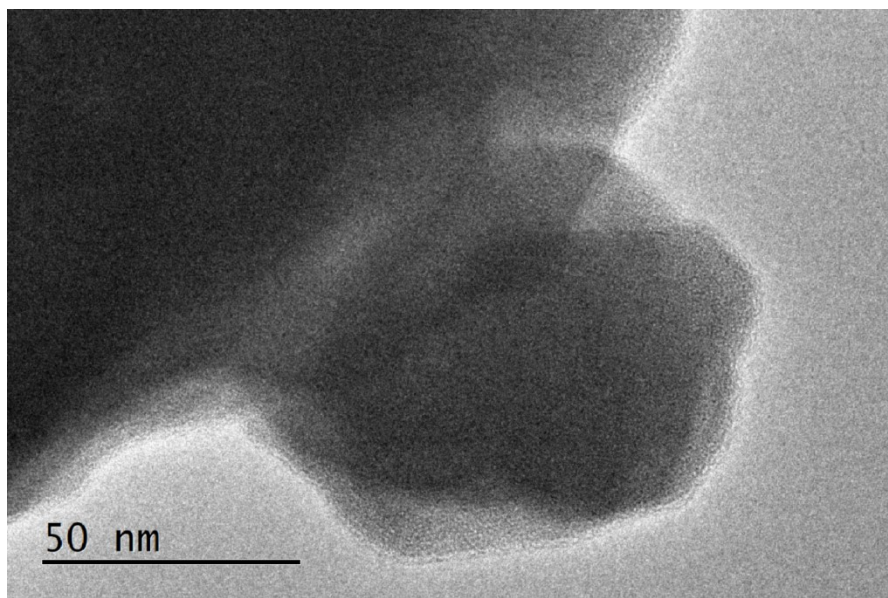


**Fig. S3.** HRTEM image of pure APMo after a few seconds. The lattice fringes disappear.

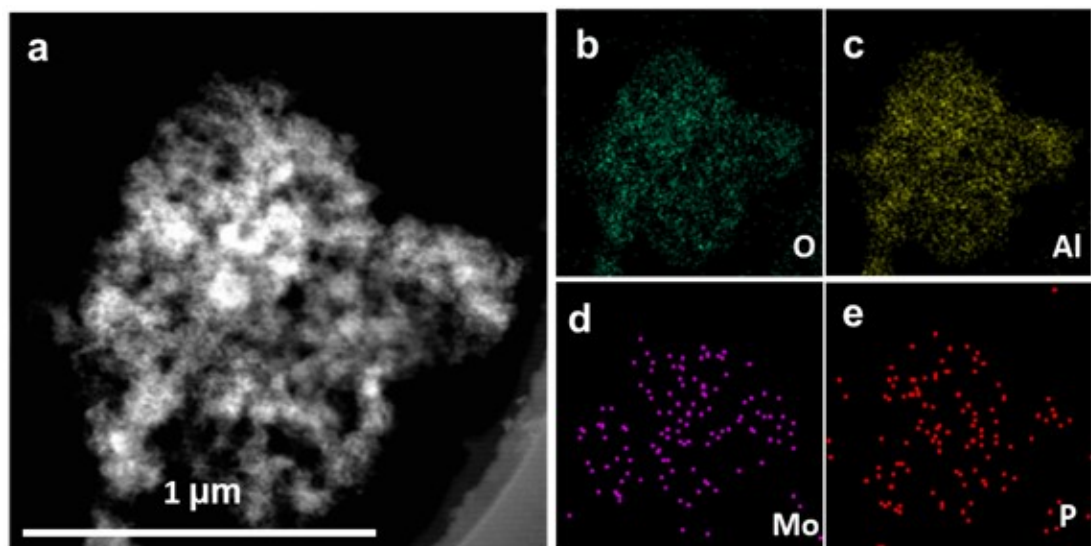


**Fig. S4.** (a-e) HAADF-STEM image and corresponding EDS maps of 12%APMo@Al<sub>rp</sub> for O, Al, P, and Mo.

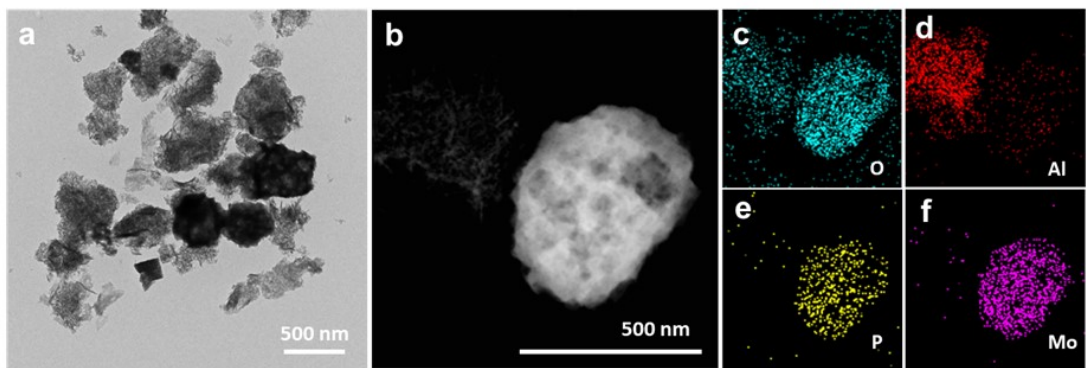


**Fig. S5.** (a)TEM image of 49%APMo/Al<sub>2</sub>O<sub>3</sub>-IM, (b-f) HAADF-STEM image and corresponding EDS maps of 49%APMo/Al<sub>2</sub>O<sub>3</sub>-IM for O, Al, P, and Mo.

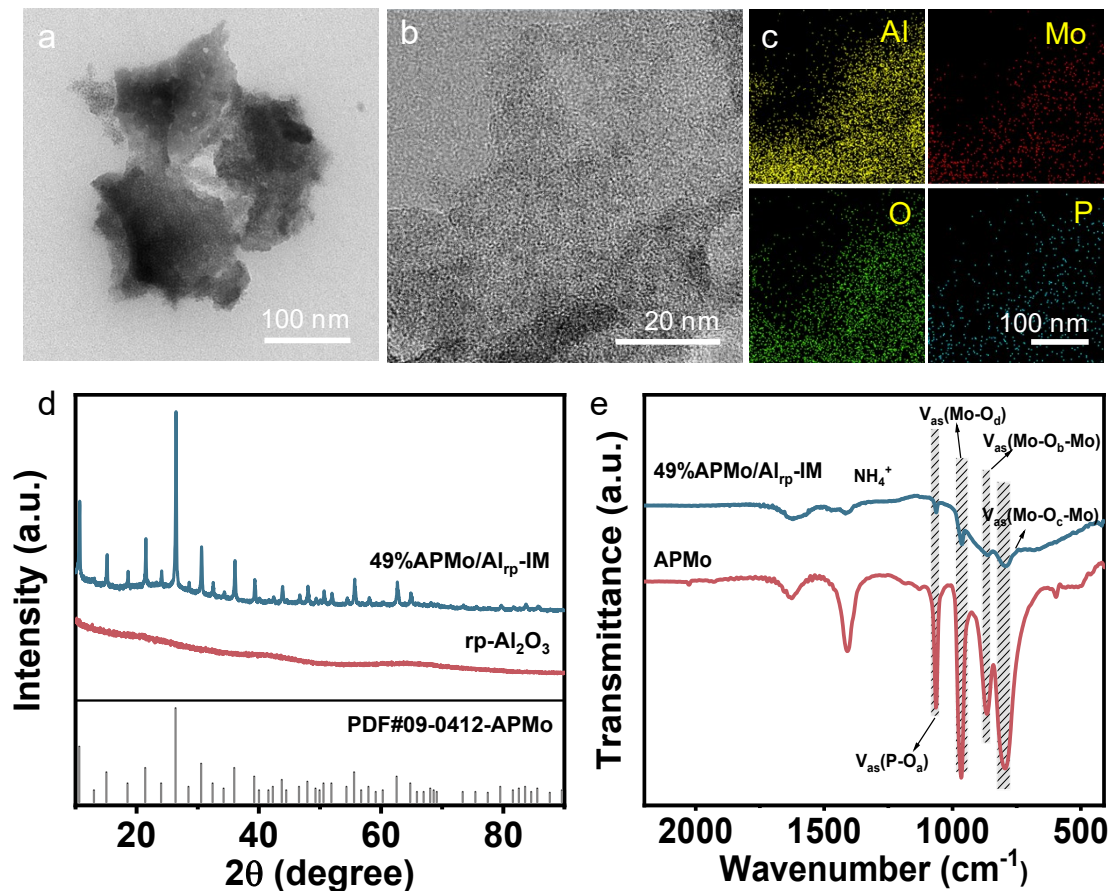


**Fig. S6.** (a)TEM, (b) HRTEM images, and (c) EDS maps of 49%APMo/Al<sub>rp</sub>-IM for Al, Mo, O, and P. (d) XRD patterns and (e) FT-IR spectra of 49%APMo/Al<sub>rp</sub>-IM.

49%APMo/Al<sub>rp</sub>-IM exhibits irregular morphology with uniform distribution of Al, O, Mo, and P elements. Powder X-ray diffraction (XRD) shows peaks assigned to the parent crystalline APMo (JCPDS No. 09-0412), proving the successful loading of APMo along with the FT-IR results exhibiting finger-print peaks of APMo.

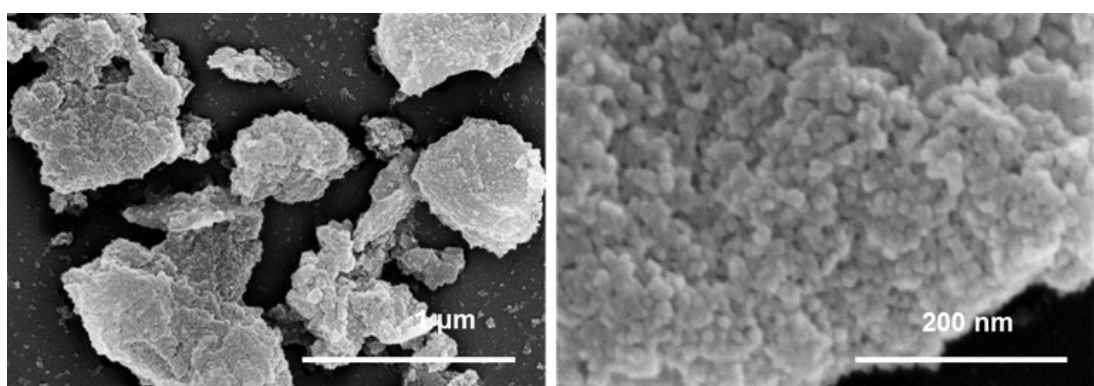


**Fig. S7.** SEM images of rp-Al<sub>2</sub>O<sub>3</sub>.

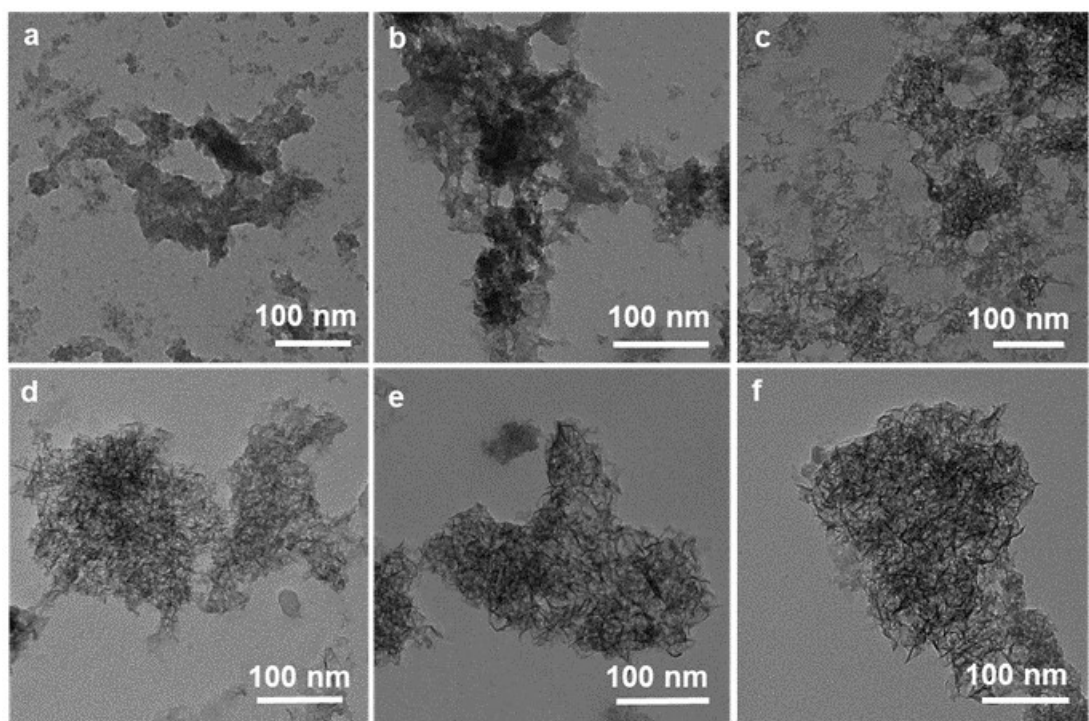


**Fig. S8.** TEM images of n%APMo@Al<sub>rp</sub> (n=0, 2, 6, 15, 38, 49).

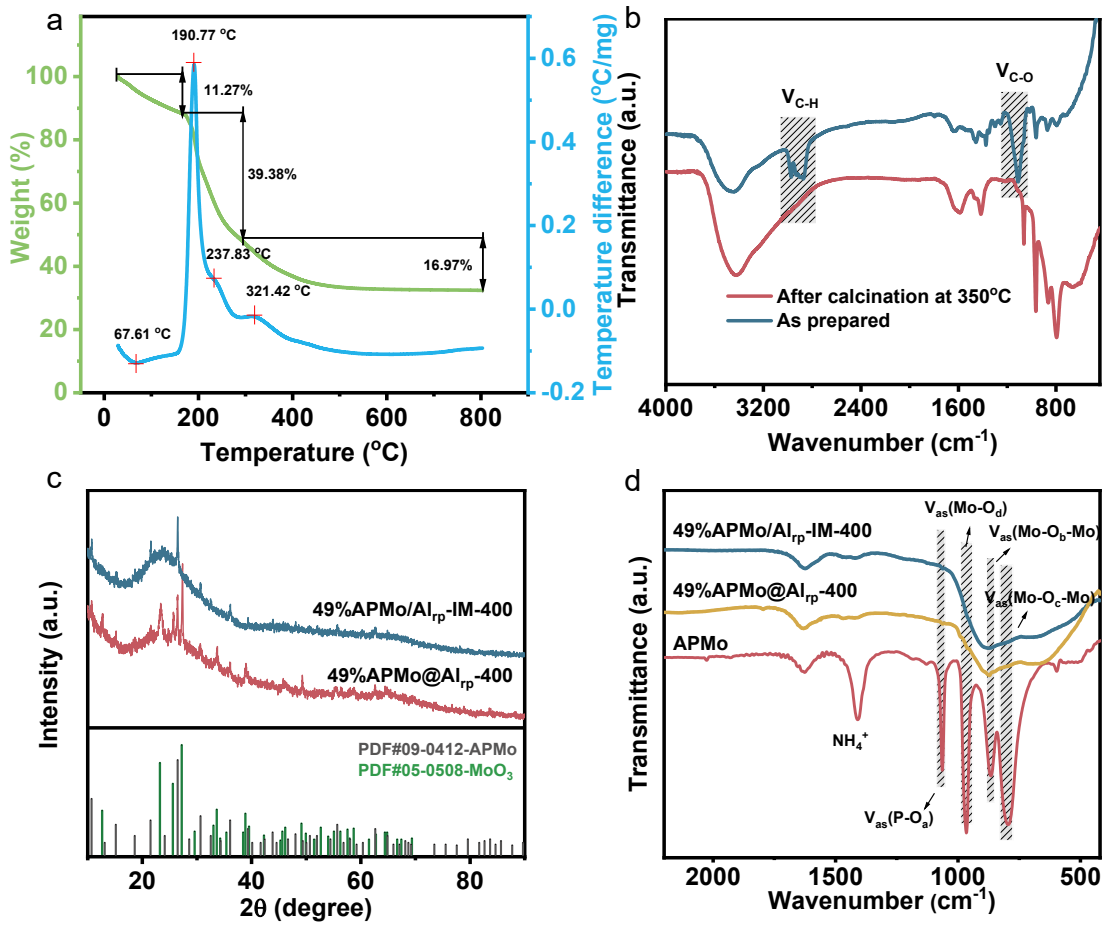


**Fig. S9.** (a) TGA-DTA curves of as-prepared 49%APMo@Al<sub>rp</sub>. (b) FT-IR spectra of as-prepared and calcined 49%APMo@Al<sub>rp</sub>. XRD patterns (c) and FT-IR spectra (d) of 49%APMo@Al<sub>rp</sub> and 49%APMo/Al<sub>rp</sub>-IM calcined at 400 °C.

The obvious exothermic peaks at 190.77 °C and 237.83 °C are attributed to the composition of P123, accompanied with significant weight loss (**Fig. S9a**). After calcination at 350 °C, the identical C-O stretching vibration bands (1000-1125 cm<sup>-1</sup>) and C-H symmetrical and asymmetric stretching vibration bands (2876 and 2930 cm<sup>-1</sup> respectively) of isopropanol and P123 disappeared<sup>1</sup> (**Fig. S9b**), implying the removal of isopropanol and P123. Further increasing the calcination temperature to 400 °C, APMo would decompose to produce MoO<sub>3</sub> species (**Fig. S9c**), with the disappearance of FT-IR finger-print peaks (**Fig. S9d**).

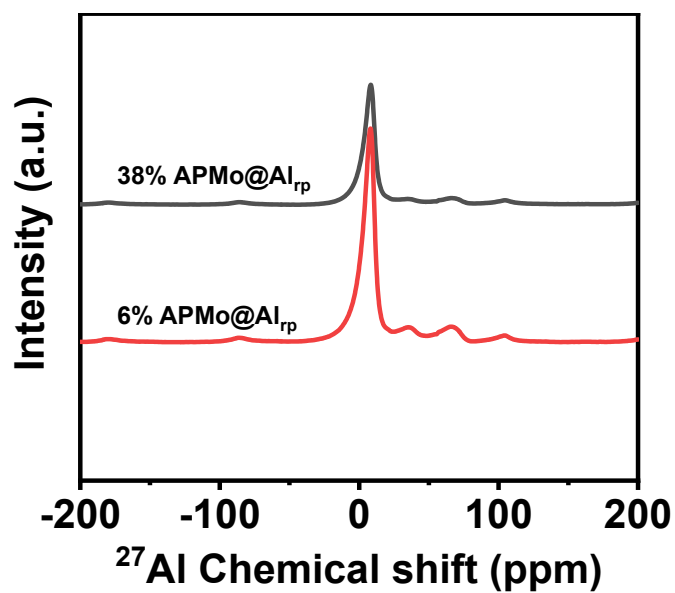


**Fig. S10.**  $^{27}\text{Al}$  MAS NMR spectra of 6%APMo@Al<sub>rp</sub> and 38%APMo@Al<sub>rp</sub>.

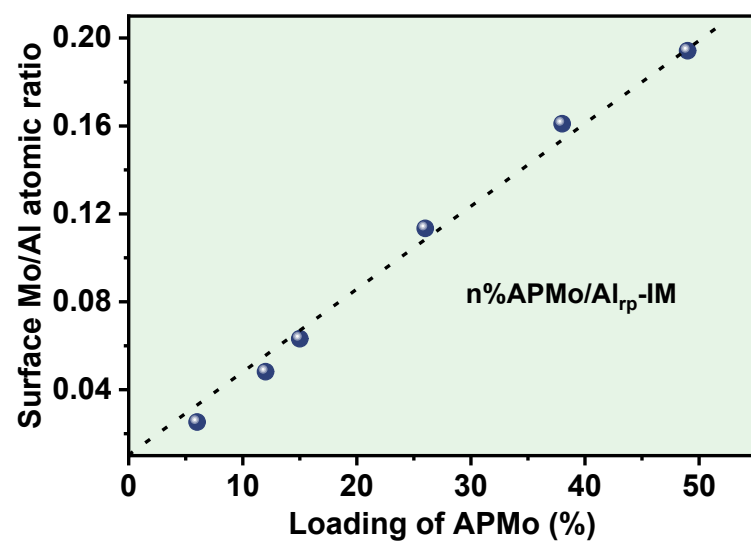


**Fig. S11.** XPS-measured surface Mo/Al atomic ratios of n%APMo/Al<sub>rp</sub>-IM.

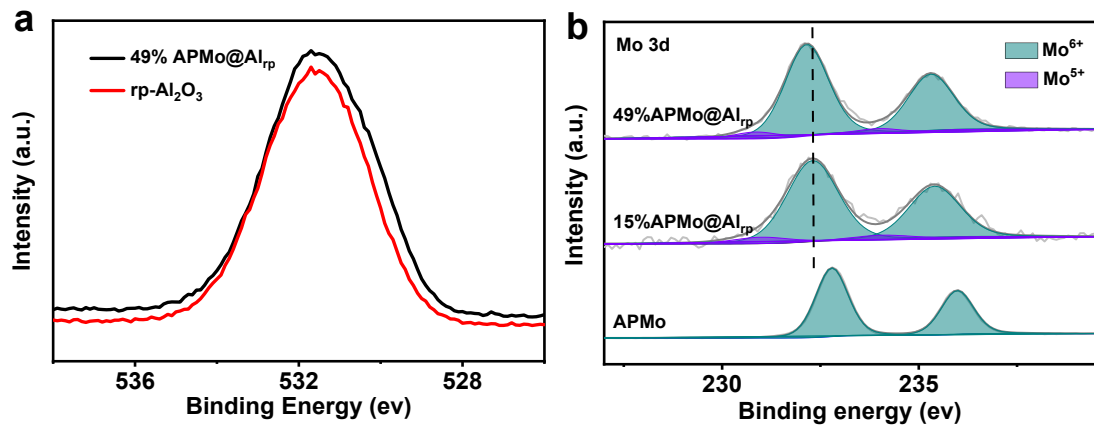


**Fig. S12.** (a-b) XPS spectra of 49%APMo@Al<sub>rp</sub>, 15%APMo@Al<sub>rp</sub>, APMo, and rp- Al<sub>2</sub>O<sub>3</sub>. High-resolution spectra for the O 1s peak (a), Mo 3d peak (b).

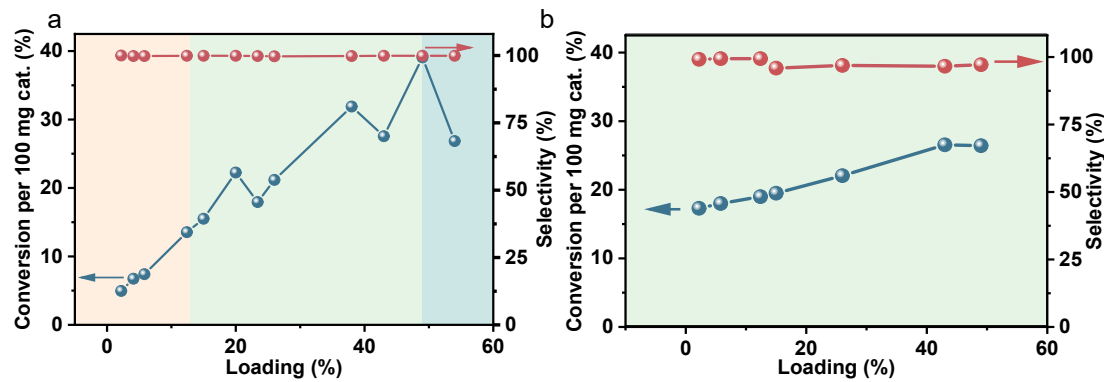


**Fig. S13.** (a-b) Conversion and selectivity of benzyl alcohol oxidation per 100 mg catalyst for n%APMo@Al<sub>rp</sub> (a), and n%APMo/Al<sub>2</sub>O<sub>3</sub>-IM (b) as a function of APMo loading (%). Reaction conditions: 100 mg catalyst, 5 mL CH<sub>3</sub>CN, 3.10 mL 30% H<sub>2</sub>O<sub>2</sub>, 2 mmol Benzyl alcohol, 80 °C, 4 h.

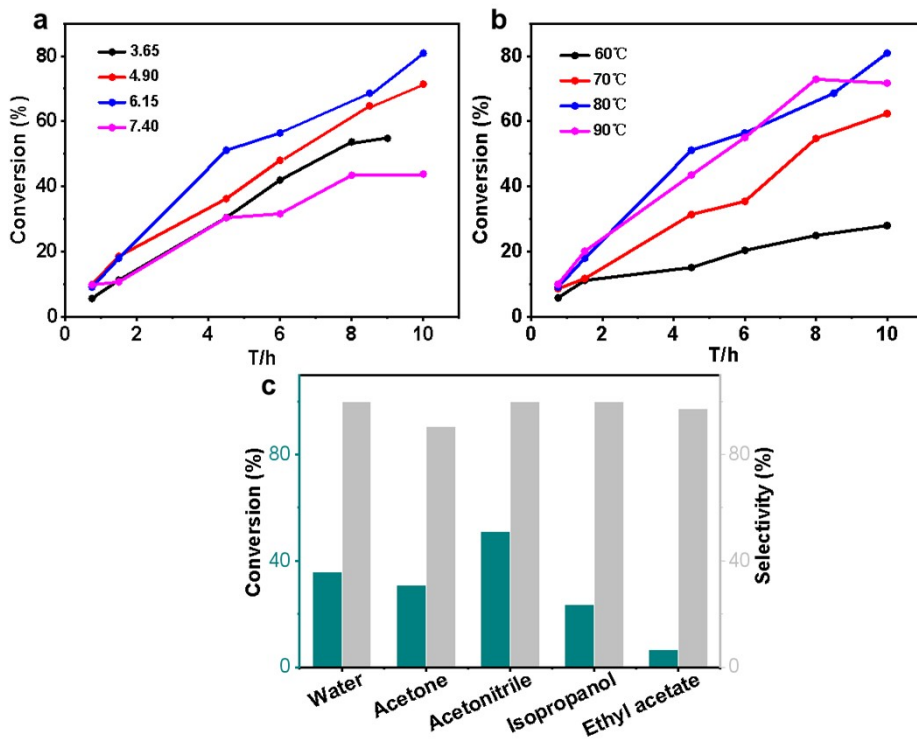


**Fig. S14.** Conversion of benzyl alcohol oxidation versus time with different volume of 30%H<sub>2</sub>O<sub>2</sub> (a) and different temperatures (b) with 49%APMo@Al<sub>rp</sub>, (c) conversion and selectivity with different solvents.

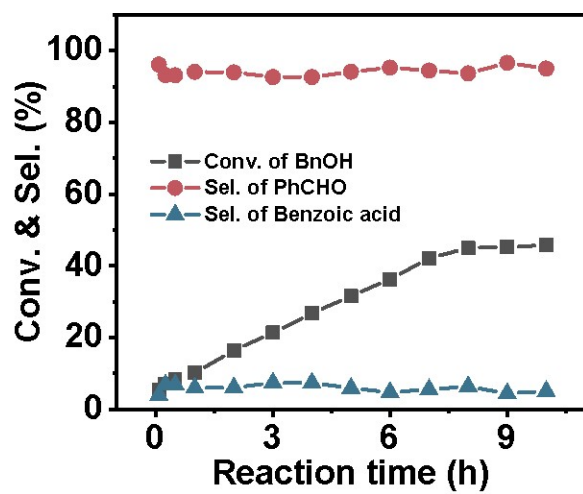


**Fig. S15.** Reaction kinetic curves of 49%APMo/Al<sub>rp</sub>-IM. Reaction conditions: 100 mg catalyst, 5 mL CH<sub>3</sub>CN, 6.15 mL 30% H<sub>2</sub>O<sub>2</sub>, 4 mmol Benzyl alcohol, 80 °C, 10 h.

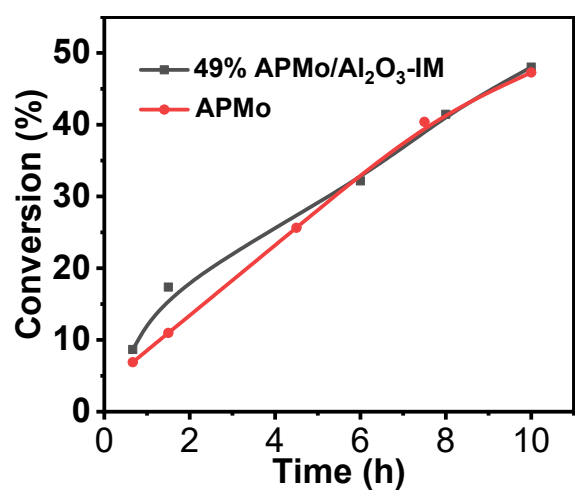


Fig. S16. Reaction kinetics curve of 49%APMo/Al<sub>2</sub>O<sub>3</sub>-IM and pure APMo.

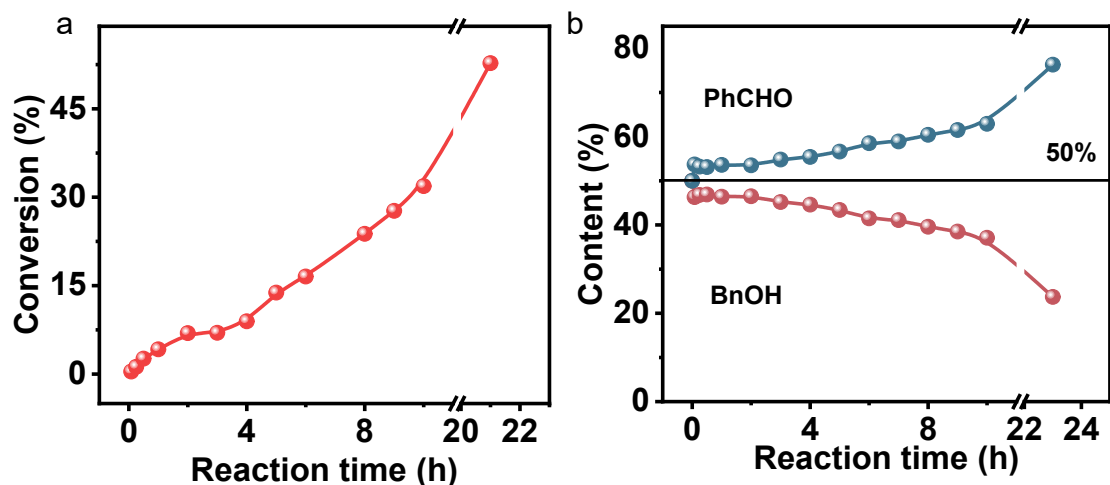
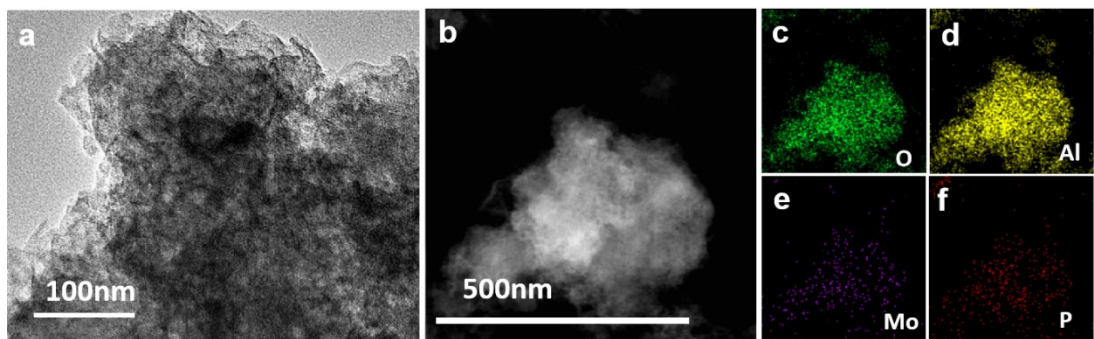
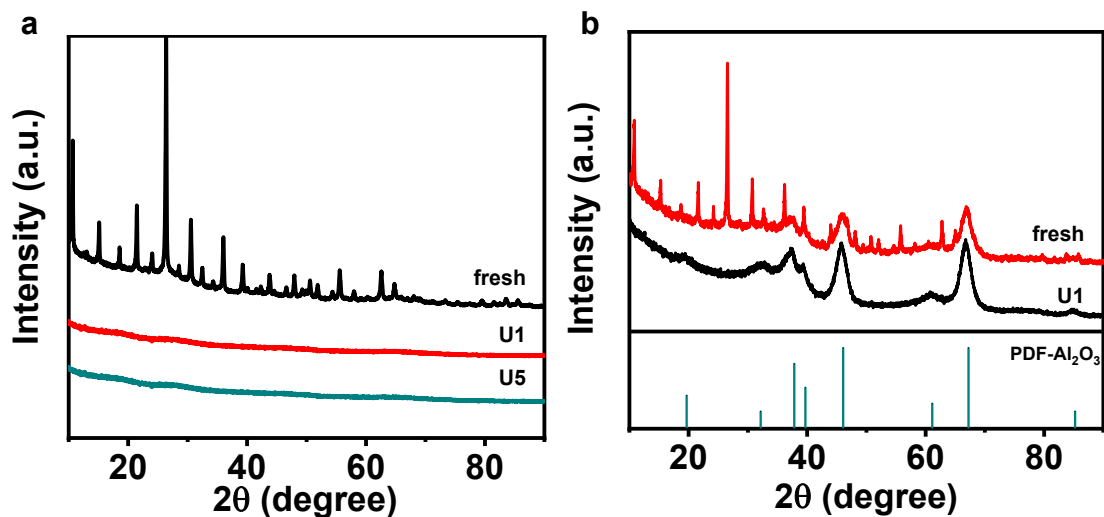


Fig. S17. Reaction kinetic curves of 49%APMo@Al<sub>rp</sub> using pure PhCHO (a) and a mixture of BnOH/PhCHO in a 50/50 ratio (b) as substrates. Reaction conditions: 100 mg catalyst, 5 mL CH<sub>3</sub>CN, 6.15 mL 30% H<sub>2</sub>O<sub>2</sub>, 4 mmol substrates, 80 °C, 21 h/23 h.



**Fig. S18.** (a)TEM image of 49%APMo@ $\text{Al}_{\text{rp}}$ -U5, (b-f) HAADF-STEM image and corresponding EDS maps of 49%APMo@ $\text{Al}_{\text{rp}}$ -U5 for O, Al, P, and Mo.



**Fig. S19.** (a) XRD patterns of fresh and reused 49%APMo@ $\text{Al}_{\text{rp}}$ , (b) XRD patterns of fresh 49%APMo/ $\text{Al}_2\text{O}_3$ -IM and 49%APMo/ $\text{Al}_2\text{O}_3$ -IM-U1.

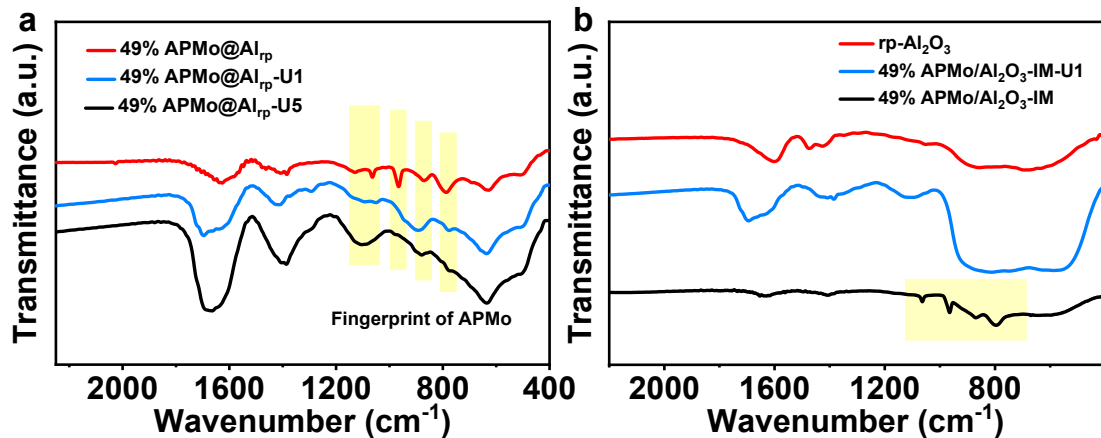


**Fig. S20.** (a) FT-IR spectra of 49%APMo@Al<sub>rp</sub> and reused samples, (b) FT-IR spectra of rp-Al<sub>2</sub>O<sub>3</sub>, 49%APMo/Al<sub>2</sub>O<sub>3</sub>-IM, and 49%APMo/Al<sub>2</sub>O<sub>3</sub>-IM-U1.

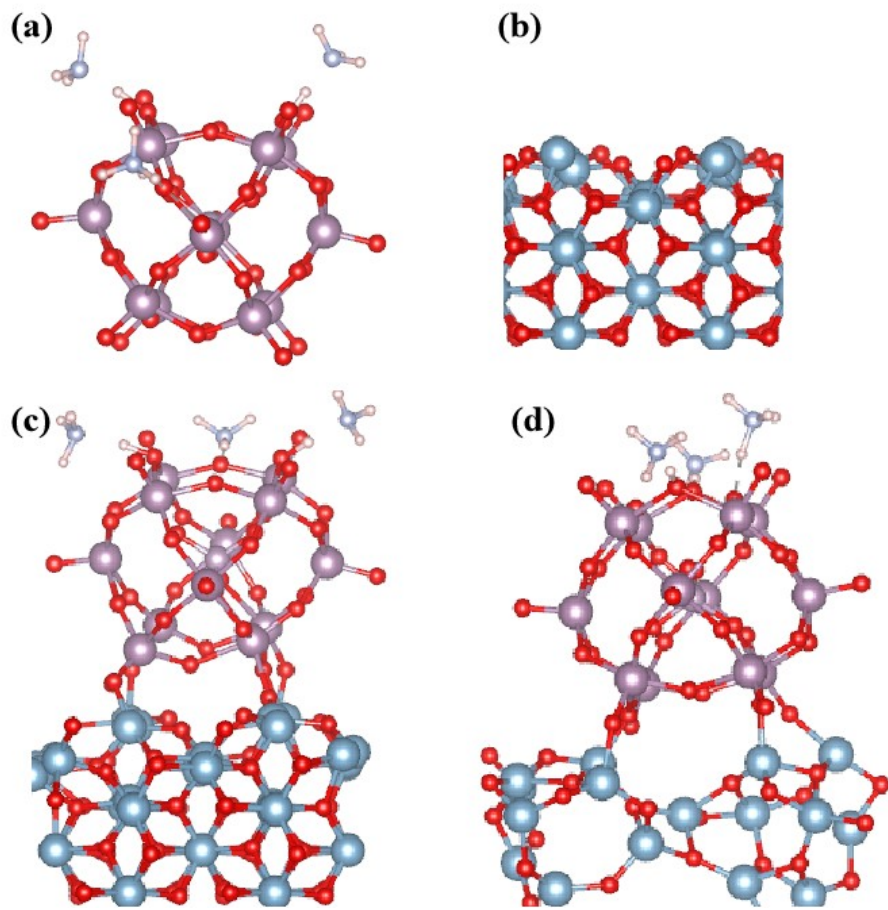


**Fig. S21.** (a-b) Catalyst structures of APMo (a),  $\text{Al}_2\text{O}_3$ -com (b), APMo/ $\text{Al}_2\text{O}_3$ -IM(c) and APMo@ $\text{Al}_{\text{rp}}$ (d).

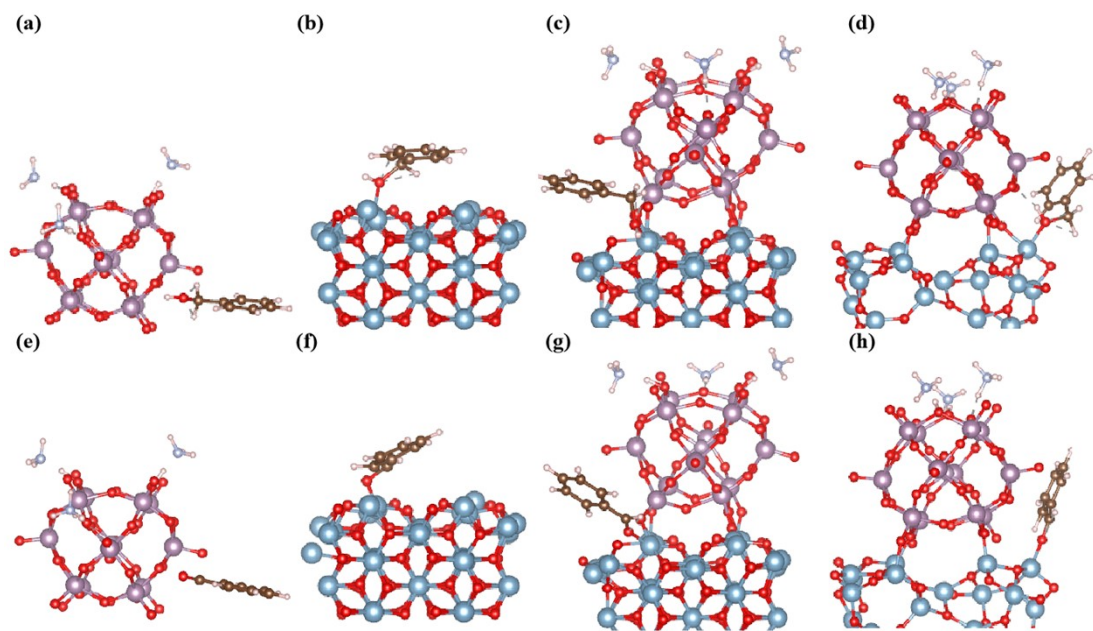


**Fig. S22.** Typical binding geometries of Benzyl alcohol (a-d) and Benzaldehyde (e-h) on different catalysts.

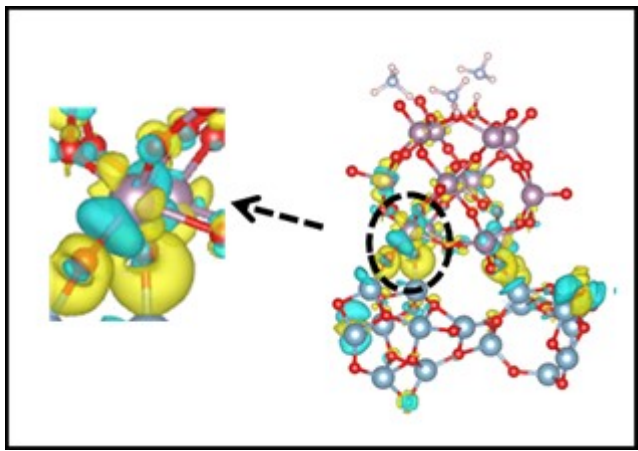


**Fig. S23.** The charge density difference between the POM and the amorphous  $\text{Al}_2\text{O}_3$  surfaces, (dark purple: Mo, light purple: P, silver: Al, red: O, blue: N, and white: H), the yellow and blue colors indicate electron accumulation and depletion, respectively, the value of the iso-surfaces was set to  $\pm 0.003 \text{ e/Bohr}^3$ .

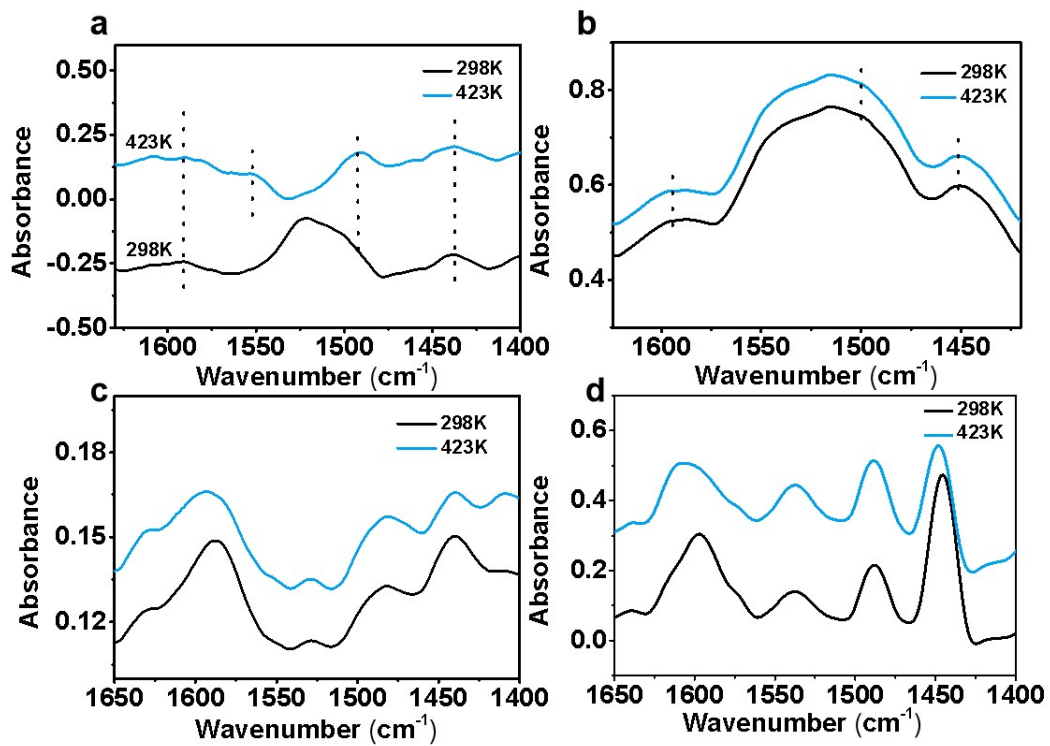


**Fig. S24.** In situ FTIR of pyridine adsorption profiles of rp-Al<sub>2</sub>O<sub>3</sub> (a), 15% APMo@Al<sub>rp</sub> (b), commercial Al<sub>2</sub>O<sub>3</sub> (c), and 49%APMo/Al<sub>2</sub>O<sub>3</sub>-IM (d).

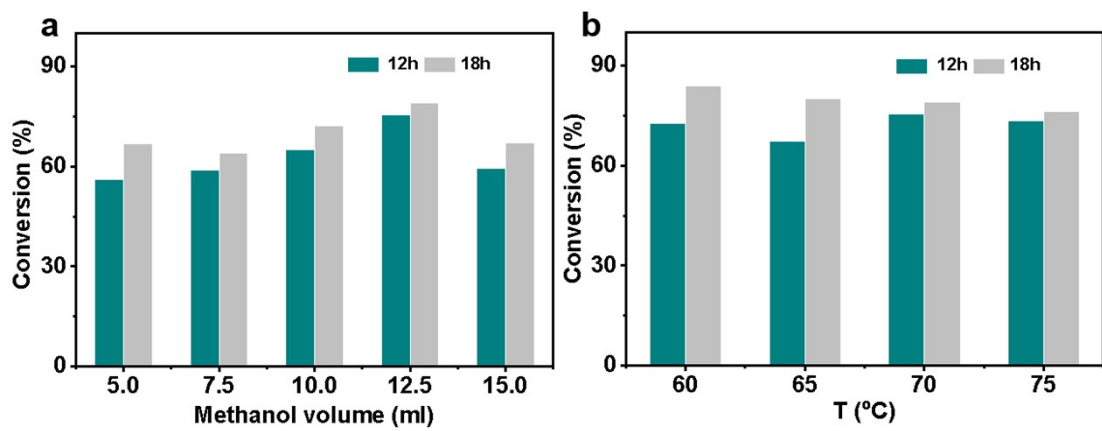


**Fig. S25.** Conversion of palmitic acid upon esterification with different volume of methanol (a), and different temperatures (b) catalyzed by 49%APMo@Al<sub>rp</sub>.

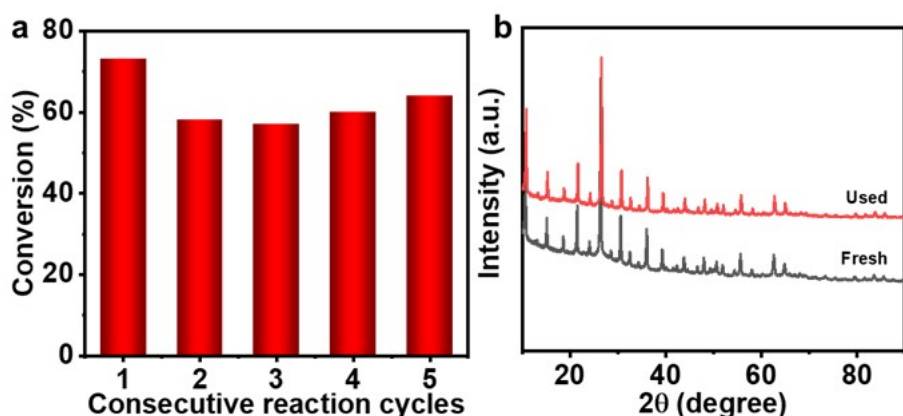


**Fig. S26.** (a) Conversion of palmitic acid esterification over consecutive reaction cycles with 49%APMo@Al<sub>rp</sub>, (b) XRD patterns of fresh and reused 49%APMo@Al<sub>rp</sub>.

**Table S1.** Physical-chemical properties of the catalysts.

Sample	$S_{\text{BET}}$ ( $\text{m}^2/\text{g}$ )	Total pore volume ( $\text{cm}^3/\text{g}$ )	Average pore diameter (nm)
rp-Al <sub>2</sub> O <sub>3</sub>	567	0.637	4.49
6%APMo@Al <sub>rp</sub>	640	0.842	5.27
15%APMo@Al <sub>rp</sub>	560	0.533	3.81
26%APMo@Al <sub>rp</sub>	518	0.499	3.85
49%APMo@Al <sub>rp</sub>	339	0.456	5.37
49%APMo/Al <sub>rp</sub> -IM	217	0.134	2.48
Al <sub>2</sub> O <sub>3</sub> -com	135	0.802	23.80
49%APMo/Al <sub>2</sub> O <sub>3</sub> -IM	124	0.528	17.93

**Table S2.** ICP-AES results of APMo loading for n%APMo@Al<sub>rp</sub>.

Catalysts	Actual loading/%
2%APMo@Al <sub>rp</sub>	2.2
4%APMo@Al <sub>rp</sub>	4.1
6%APMo@Al <sub>rp</sub>	5.8
12%APMo@Al <sub>rp</sub>	12.4
15%APMo@Al <sub>rp</sub>	15.0
23%APMo@Al <sub>rp</sub>	23.4
20%APMo@Al <sub>rp</sub>	19.8
26%APMo@Al <sub>rp</sub>	25.54
38%APMo@Al <sub>rp</sub>	38.0
43%APMo@Al <sub>rp</sub>	42.6
49%APMo@Al <sub>rp</sub>	48.7
54%APMo@Al <sub>rp</sub>	54.1

**Table S3.** <sup>27</sup>Al MAS Percentage of aluminum with different coordination numbers.

Entry	Catalysts	Al <sub>T</sub> /%	Al <sub>p</sub> /%	Al <sub>o</sub> /%
1	rp-Al <sub>2</sub> O <sub>3</sub>	11	15	74
2	6%APMo@Al <sub>rp</sub>	10	10	80
3	15%APMo@Al <sub>rp</sub>	12	20	68
4	38%APMo@Al <sub>rp</sub>	8	9	83
5	49%APMo@Al <sub>rp</sub>	7	2	91

**Table S4.** ICP-AES results of 49%APMo@Al<sub>rp</sub> and the used ones.

Entry	Catalysts	APMo loading/%
1	49%APMo@Al <sub>rp</sub>	48.7
2	49%APMo@Al <sub>rp</sub> -U5 <sup>a</sup>	34.3
3	49%APMo@Al <sub>rp</sub> -U5 <sup>b</sup>	37.0
4	49%APMo@Al <sub>rp</sub> <sup>c</sup>	45.8

a: after five cycles of benzyl alcohol oxidation;

b: after five cycles of palmitic acid esterification;

c: after repeated washing with water.

**Table S5.** Comparison of results obtained over different Keggin-type POM catalysts in the selective oxidation of benzyl alcohol with H<sub>2</sub>O<sub>2</sub>.

Entry	Catalyst	Reaction	Reaction	Mol ratio	Mol ratio	Conv.	Sel.	Ref.
		Time(h)	Temperature(°C)	(H <sub>2</sub> O <sub>2</sub> /alc ohol)	(Alcohol/cat)	(%)	(%)	
1	49%APMo@Al <sub>rp</sub>	10	80	15	155	81	100	This work
2	{3CD@SiW <sub>12</sub> }	24	85	5	250	96	25	2
3	[SiW <sub>12</sub> O <sub>40</sub> ] <sup>4-</sup>	24	85	5	250	19	15.8	2
4	[PW <sub>12</sub> O <sub>40</sub> ] <sup>3-</sup>	6	95	1.5	77	48	67	3
5	[PW <sub>11</sub> ZnO <sub>39</sub> ] <sup>5-</sup>	8	85	10	20	34	100	4
6	[BW <sub>11</sub> O <sub>39</sub> H]	6	90	2	66.7	98	83	5
7	H <sub>5</sub> PV <sub>2</sub> W <sub>10</sub> O <sub>40</sub>	8	80	>20	2.6	75	93	6
8	PIPA-13	6	95	1.5	77	96	86	3
9	[TMGOH] <sub>2.2</sub> H <sub>0.8</sub> P W	6	90	1.5	333.3	90	89.2	7
10	[PyHA] <sub>3</sub> PW	6	90	1.5	6	72	95.8	7
11	PW-NH <sub>2</sub> -IL-SBA- 15	6	100	3.0	-	72	91	8
12	(PW <sub>11</sub> ) <sub>3</sub> /MCM-41	20	80	3.0	-	30	90	9

The amount of H<sub>2</sub>O<sub>2</sub> used in the reaction is relatively high, mainly because the support of our catalyst 49%APMo@Al<sub>rp</sub> is essentially amorphous AlOOH. AlOOH (especially AlOOH with surface defects) tends to absorb H<sub>2</sub>O<sub>2</sub> via Al-O-H structure interacting with the oxygen atom of H<sub>2</sub>O<sub>2</sub><sup>10</sup>. Besides, AlOOH has been reported to be the support material of H<sub>2</sub>O<sub>2</sub> electrochemical sensing<sup>11</sup>. The support adsorbs a large amount of H<sub>2</sub>O<sub>2</sub>, resulting in the need to provide much H<sub>2</sub>O<sub>2</sub> to ensure the formation of adequate [Mo(O)(O<sub>2</sub>)<sub>2</sub>] intermediates on APMos. The relatively high reaction temperature and high APMo loading may also account for the high H<sub>2</sub>O<sub>2</sub> dosage.

**Table S6.** Comparison of results obtained over different reported catalysts in palmitic acid esterification.

Catalyst	Reaction condition	Conv. (%)	Ref.
49%APMo@Al <sub>rp</sub>	60 °C 18 h	89	This work
49%APMo/Al <sub>2</sub> O <sub>3</sub> -IM	60 °C 18 h	47	This work
ZrO <sub>2</sub> -TiO <sub>2</sub>	100 °C 5 h	93	12
PIL-3	65 °C 10 h	91	13
SBA-15-SO <sub>3</sub> H	85 °C 3 h	85	14
Zr-SBA15-08	160 °C 6 h	64	15
ZeoA@MesoS	60 °C 50 h	75	16
Al-MCM-41	130 °C 2 h	79	17

**Table S7** Acidity properties of the catalysts.

Catalyst	Total acid site (mmol <sub>NH3</sub> /g) <sup>a</sup>	B/L ratio <sup>b</sup>
49%APMo@Al <sub>rp</sub>	2.17	0.08
49%APMo/Al <sub>rp</sub> -IM	1.75	0.15
rp-Al <sub>2</sub> O <sub>3</sub>	1.54	0.04
49%APMo/Al <sub>2</sub> O <sub>3</sub> -IM	1.30	0.56
Al <sub>2</sub> O <sub>3</sub> -com	0.31	0.24

<sup>a</sup>Determined from NH<sub>3</sub>-TPD results.

<sup>b</sup>Determined from the integral area ratios of absorbance bonds at 1543 and 1447 cm<sup>-1</sup>, respectively.

### Reference:

- [1] I. Saptiama, Y. Kaneti, Y. Suzuki, K. Tsuchiya, N. Fukumitsu, T. Sakae, J. Kim, Y. Kang, K. Ariga,

- and Y. Yamauchi, *Small*, 2018, **14**, 1800474.
- [2] L. Ni, H. Li, H. Xu, C. Shen, R. Liu, J. Xie, F. Zhang, C. Chen, H. Zhao, T. Zuo and G. Diao, *ACS Appl. Mater. Inter.*, 2019, **11**, 38708.
- [3] A. A. M. Prabhu, R. K. Sankaranarayanan, G. Venkatesh and N. Rajendiran, *J. Phys. Chem. B*, 2012, **116**, 9061.
- [4] P. Hao, M. Zhang, W. Zhang, Z. Tang, N. Luo, R. Tan and D. Yin, *Catal. Sci. Technol.*, 2018, **8**, 4463.
- [5] Z. Nadealian, V. Mirkhani, B. Yadollahi, M. Moghadam, S. Tangestaninejad and I. Mohammadpoor-Baltork, *J. Coord. Chem.*, 2013, **66**, 1264.
- [6] W. Zhao, Y. Zhang, B. Ma, Y. Ding and W. Qiu, *Catal. Commun.*, 2010, **11**, 527.
- [7] X. Dong, X. Zhang, P. Wu, Y. Zhang, B. Liu, H. Hu and G. Xue, *ChemCatChem*, 2016, **8**, 3680.
- [8] G. Chen, Y. Zhou, Z. Long, X. Wang, J. Li and J. Wang, *ACS Appl. Mater. Inter.*, 2014, **6**, 4438.
- [9] R. Tan, C. Liu, N. Feng, J. Xiao, W. Zheng, A. Zheng and D. Yin, *Micropor. Mesopor. Mater.*, 2012, **158**, 77.
- [10] A. Sharipov, A. Starik, *Chem. Phys.*, 2016, **465**, 9.
- [11] Z. Yang, C. Qi, X. Zheng, J. Zheng, *J. Electroanal. Chem.*, 2015, **754**, 138.
- [12] M. Fan, Z. Si, W. Sun and P. Zhang, *Fuel*, 2019, **252**, 254-.
- [13] Y. Wang, D. Zhao, G. Chen, S. Liu, N. Ji, H. Ding, and J. Fu, *Renew. Energ.*, 2019, **133**, 317e324.
- [14] Isa K. Mbaraka, Daniela R. Radu, Victor S.-Y. Lin, and Brent H. Shanks, *J. Catal.*, 2003, **219**, 329.
- [15] Vahide Nuran Mutlu, Selahattin Yilmaz, *Appl. Catal. A.*, 2016, **522**, 194.
- [16] C. Hung, L. Duan, T. Zhao, L. Liu, Y. Xia, Y. Liu, P. Qiu, R. Wang, Z. Zhao, W. Li, and D. Zhao, *J. Am. Chem. Soc.* 2022, **144**, 6091.
- [17] Alípio C. Carmo Jr, Luiz K.C. de Souza, Carlos E.F. da Costa, E. Longo, José R. Zamian, Geraldo N. da Rocha Filho, *Fuel*, 2009, **88**, 461.